Magnetic resonance imaging techniques for risk stratification in cardiovascular disease

Roes, S.D.

Chapter

2

Aortic vessel wall magnetic resonance imaging at 3 tesla

A reproducibility study of respiratory navigator gated free-breathing 3D black-blood magnetic resonance imaging

S.D. Roes
J.J.M. Westenberg
J. Doornbos
R.J. van der Geest
E. Angelié
A. de Roos
M. Stuber

Abstract

The purpose of this study was to evaluate a free-breathing three-dimensional (3D) dual inversion recovery (DIR) segmented k-space gradient echo (turbo field echo [TFE]) imaging sequence at 3T for the quantification of aortic vessel wall dimensions. The effect of respiratory motion suppression on image quality was tested. Furthermore, the reproducibility of the aortic vessel wall measurements was investigated. Seven healthy subjects underwent 3D DIR TFE imaging of the aortic vessel wall with and without respiratory navigator. Subsequently, this sequence with respiratory navigator was performed twice in 10 healthy subjects to test its reproducibility. Signal-to-noise (SNR), contrast-to-noise ratio (CNR), vessel wall sharpness, and vessel wall volume (VWV) were assessed. Data were compared using the paired t-test and the reproducibility of VWV measurements was evaluated using intraclass correlation coefficients (ICCs). SNR, CNR, and vessel wall sharpness were superior in scans performed with respiratory navigator compared to scans performed without. The ICCs concerning intraobserver, interobserver, and interscan reproducibility were excellent (0.99, 0.94, and 0.95, respectively). In conclusion, respiratory motion suppression substantially improves image quality of 3D DIR TFE imaging of the aortic vessel wall at 3T. Furthermore, this optimized technique with respiratory motion suppression enables assessment of aortic vessel wall dimensions with high reproducibility.

Introduction

Atherosclerosis is regarded as a chronic systemic disease of the vessel wall that occurs in the peripheral arteries, the coronary arteries, and the aorta (1). Autopsy studies and in vivo studies reported a strong association between thoracic aortic atherosclerosis and coronary artery disease (CAD)(2,3). Consequently, imaging of (subclinical) aortic atherosclerosis may provide a valuable measure of cardiovascular risk (4).

High-spatial-resolution imaging of the vessel wall would allow for detection of the early stage of atherosclerosis, that is, outward arterial remodeling (Glagov phenomenon), which precedes luminal narrowing (5). Furthermore, high-spatial-resolution imaging allows for evaluation of disease progression and assessment of the effect of therapeutic agents on aortic vessel wall thickness (VWT) using a relatively small sample size (6).

Thus, a reproducible technique for vessel wall imaging able to detect small changes in aortic vessel wall dimensions is clinically highly desirable.

Magnetic resonance imaging (MRI) allows for imaging of the aortic vessel wall, with good reproducibility on 1.5 Tesla (T) MR systems (7,8). The recent introduction of clinical 3T MRI systems enables imaging at higher spatial resolution (9). However, imaging with improved spatial resolution necessitates adequate motion supression strategies, since the aorta is subject to intrinsic and extrinsic motion. Data acquisition during diastole after passage of the arterial pulse wave (using electrocardiographic [ECG] triggering) can account for intrinsic aortic motion (8,10). Extrinsic aortic motion is attributable to respiration. While all previous 1.5T MRI aortic wall studies acquired data during free-breathing, 3T imaging in conjunction with navigator technology (11,12) to suppress respiratory motion artefacts may support reproducible high-spatial-resolution imaging of the aortic vessel wall.

Koops et al. (13) demonstrated that imaging at 3T offers superior plaque imaging quality compared to at 1.5T. However, this was an ex vivo study, and in vivo studies describing 3T MRI for aortic vessel wall imaging are scarce (14,15).

To our knowledge, no in vivo studies have been published yet describing 3T MRI for the measurement of the aortic vessel wall dimensions.

Accordingly, the aim of this study was the implementation of a free-breathing three-dimensional (3D) dual inversion recovery (DIR) segmented k-space gradient echo (turbo field echo [TFE]) imaging sequence at 3T for the quantification of aortic vessel wall dimensions. The effect of respiratory motion suppression on image quality was evaluated. Furthermore, we investigated the reproducibility of the aortic vessel wall measurements acquired with this optimized, respiratory motion-suppressed technique.

Materials and methods

Study population

Seventeen healthy adult subjects without a prior history of cardiovascular disease were enrolled in the study. In 7 subjects (3 males and 4 females, mean age 26 ± 7 years), aortic MRI was performed with and without respiratory navigator during one MRI examination, in order to study the effect of the respiratory motion suppression on image quality. Furthermore, 10 subjects (7 males and 3 females, mean age 23 ± 4 years) underwent two aortic MRI examinations to test the reproducibility. After the first examination, the study subjects were removed from the scanner, the surface coil was removed, and the subjects were repositioned and the complete examination was repeated. Informed consent was obtained from each subject and the protocol was approved by the hospital's medical ethics committee.

MRI Protocol

MRI studies were performed on a clinical 3T System (Achieva; Philips Medical Systems, Best, The Netherlands) using a 6-element cardiac phased-array surface coil for signal reception. The study subjects were positioned in the supine position and data were acquired using vector ECG gating. Second-order shimming and F_0 determination was performed using a localized shimming tool that was implemented on a personal computer using IDL (Research systems, Inc., Boulder, CO, USA) and connected to the scanner database (16).

The 3D cross-sectional acquisition for assessment of the aortic vessel wall was planned following a standardized scan protocol (described below) to ensure that the same segment of the aortic vessel wall was imaged during both the first and second examination (in order to test reproducibility). The scan protocol is illustrated in Figure 1, describing the localization steps and anatomic landmarks that were used as fiducial markers.

First, a survey scan of the thorax was obtained using an ECG-triggered segmented k-space gradient echo imaging sequence with three stacks in three spatial orientations (coronal, sagittal, and axial plane) and 20 slices per stack. The scan parameters were as follows: field of view (FOV) of 450 × 450 mm^2, acquisition matrix of 256 × 256 pixels, slice thickness of 5.0 mm, flip angle (α) of 15°, echo time (TE) of 2.5 ms, and repetition time (TR) of 5.0 ms. Data were acquired in diastole to minimize flow artifacts.

A second survey scan was performed at the level of the cervical spine in the sagittal orientation with an ECG-triggered segmented k-space gradient echo imaging sequence using the body coil for signal reception. The cervical vertebrae were used as fiducial markers to define a segment of the aorta. Ten slices of 7 mm thickness were acquired with FOV of 450 × 450 mm^2, acquisition matrix of 256 × 256 pixels, α of 15°, TE of 2.3 ms, and TR of 4.7 ms.
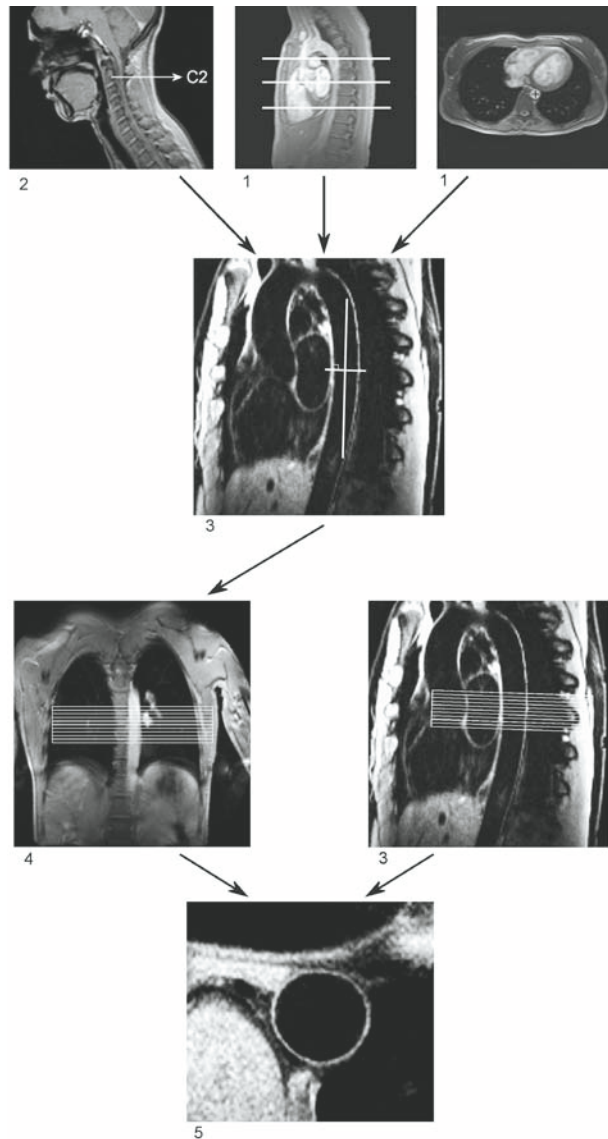
Figure 1.

Illustration of the scan protocol for assessment of the aortic vessel wall.
The first and the second surveys (1 and 2 in figure) were used to identify the 6th, 8th, and 10th thoracic vertebrae. The third survey was planned by defining three points (three-point plan scan tool) in the center of the thoracic aorta at the level of the upper edges of these three vertebrae, resulting in a double oblique sagittal view of the aorta (3 in figure). The fourth survey was planned perpendicular to the vessel wall at the level of the 8th thoracic vertebra, which resulted in a double oblique coronal view of the aorta (4 in figure). The final 3D volume for high-spatial-resolution assessment of the aortic vessel wall was planned perpendicular to the vessel wall in the double oblique coronal and double oblique sagittal view of the aorta. The upper side of the slab was placed at the level of the upper edge of the 8th thoracic vertebra. This resulted in a cross-sectional view aortic vessel wall (5 in figure).

The third survey scan was localized by defining three points (three point-planscan tool (17)) in the center of the descending aorta on the images of the first survey scan. These three points were localized at the level of the cranial border of the 6th, 8th, and 10th thoracic vertebrae. This resulted in a double oblique sagittal view of the aorta. For this scan, an ECG-triggered (end-diastole) DIR (black-blood)(18), segmented k-space gradient echo imaging sequence with fat suppression was used to maximize contrast between aortic wall, blood and perivascular fat. The DIR prepulse consisted of two nonadiabatic inversion pulses: a non-selective inversion of the magnetization, followed by a slice-selective reinversion. Data were acquired during free-breathing using a prospective 2D selective navigator localized at the dome of the right hemidiaphragm using a 5-mm gating window. One slice of 5 mm was acquired and a reinversion slice thickness of 7 mm was used. The scan parameters were as follows: FOV of 360 × 270 mm^2, acquisition matrix of 512 × 512 pixels, α of 20°, TE of 5.1 ms, and TR of 10 ms. The heart rate-dependent time delay between the dual inversion prepulse and the data acquisition was adjusted for maximized blood-signal suppression using the Fleckenstein formula (19). Data were acquired every other heartbeat to minimize the likelihood of slow-flowing blood leading to artifactual signal enhancement at the periphery of the vessel lumen.

The fourth survey scan was then localized perpendicular to the aortic vessel wall (at the level of the 8th thoracic vertebra) on the image of the third survey. This resulted in a double oblique coronal view of the thoracic descending aorta. For this scan, an ECG-triggered (end-diastole) segmented k-space gradient echo imaging sequence was used. The scan parameters were as follows: FOV of 450 × 450 mm^2, acquisition matrix of 256 × 192 pixels, α of 15°, TE of 2.3 ms, TR of 4.7 ms, and 2 signal averages (NSA).

For the final high-spatial-resolution, cross-sectional acquisition of the aortic vessel wall, an ECG-triggered (end-diastole) 3D DIR (black-blood) segmented k-space gradient echo imaging sequence with fat suppression was used. Again, nonadiabatic pulses for the dual inversion were utilized. Data acquisition was repeated during free-breathing, with and without respiratory motion suppression for comparison. For respiratory motion suppression, a right hemidiaphragmatic two-dimensional (2D) selective navigator with a 5-mm gating window was applied in the feet-head direction. No prospective adaptive slice tracking was applied (20). A schematic view of the individual sequence components is shown in Figure 2. This scan was planned perpendicular to the aortic wall on the double oblique coronal and double oblique sagittal image of the aorta (third and fourth survey scan). The upper margin of the 3D slab was localized at the level of the margin between the 8th thoracic vertebra and the intervertebral disc between the 7th and 8th vertebrae.

Figure 2.
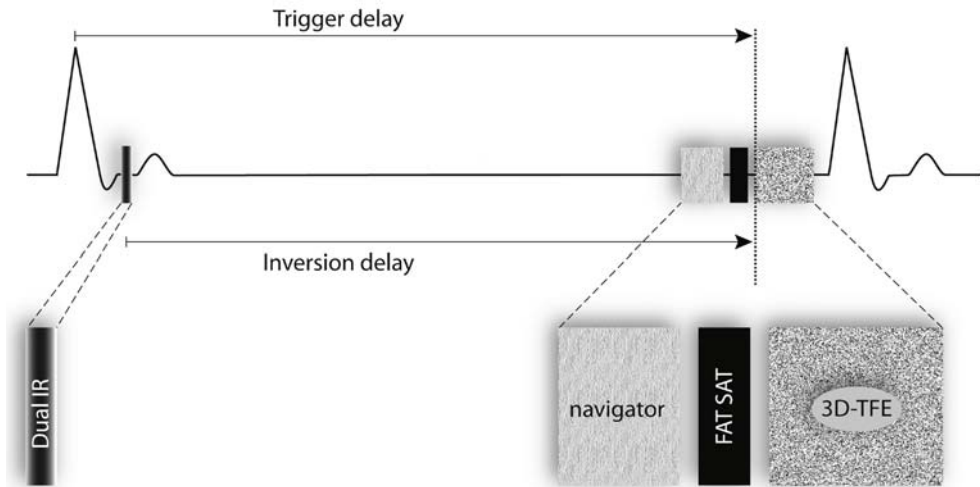
Schematic view of the sequence elements of the 3D DIR segmented *k*-space gradient echo imaging sequence. A DIR prepulse consisting of a nonselective followed by a slice selective 180° radiofrequency pulse (black-blood inversion slice of 22 mm) is applied directly after detection of the R-wave of the ECG. No adiabatic pulses were used. The navigator with a 5-mm gating window precedes the frequency-selective fat suppression (FAT SAT) and the end-diastolic 3D segmented *k*-space gradient echo imaging sequence. The inversion delay is adjusted to null magnetization of blood at the time of image data acquisition (3D-TFE). The trigger delay is used to minimize adverse effects of the pulse wave, and both dual inversion and imaging are performed in the same cardiac cycle.

This resulted in the acquisition of one 2-cm-thick cross-sectional 3D slab, with a 4-mm acquired and 2-mm reconstructed voxel slice in slice direction. Therefore, 10 slices of 2 mm were available for analysis. A reinversion slice thickness of 22 mm was used. Scan parameters included a FOV of 270 × 203 mm², acquisition matrix of 512 × 366 pixels (acquired in-plane resolution 0.53 × 0.55 mm, reconstructed in-plane resolution 0.53 × 0.53 mm), α of 20°, TE of 2.5 ms, TR of 4.9 ms and 2 NSA. The heart rate-dependent time delay between the dual inversion prepulse and the data acquisition was adjusted for maximized blood-signal suppression using the Fleckenstein formula (19) in a manner similar to the sagittal 2D black-blood image. Also, data were acquired every other heartbeat to minimize the likelihood of slow-flowing blood contributing to artifactual enhancement at the periphery of the vessel lumen.

The heart rate of the subjects and the acquisition time of the 3D cross-sectional vessel wall scans as well as the navigator efficiency were recorded.

Image analysis

Respiratory navigator

For evaluation of the effect of respiratory motion suppression on image quality, signal-to-noise ratio (SNR) and wall-lumen contrast-to-noise ratio (CNR) were measured in the sixth slice of the cross-sectional 3D vessel wall images acquired with and without respiratory navigator, using the "Soap-Bubble" tool (21). For determination of the background noise, a region of interest (ROI) was drawn in the lung instead of outside the thorax, since the FOV was chosen smaller than the cross section of the body (270 mm). This ROI was located in an area of the left lung (area without large pulmonary vessels) to avoid interference with the right hemidiaphragmatic navigator. Thus, SNR for the vessel wall was calculated by measuring the mean signal intensity in the vessel wall and dividing this by the standard deviation (SD) of the signal from the ROI in the left lung. Wall-lumen CNR was defined as the difference of the mean signal intensities in the vessel wall and an ROI in the aortic lumen divided by the SD from the ROI in the left lung. Furthermore, vessel wall sharpness was calculated with a Deriche filter (22) using the "Soap-Bubble" tool in the region where the aortic wall borders the left lung. In addition, the images were visually analyzed using the VesselMass software package (Medis, Leiden, The Netherlands) (23). First, the 3D cross-sectional vessel wall images were visually examined for the presence of respiratory artifacts. Then, the circumference of the outer wall in all analyzed slices was divided into 12 equiangular segments and the mean percentage and location of segments (average of the analyzed slices) in which the outer wall boundary could not be discriminated from neighboring tissue was evaluated in each 3D cross-sectional vessel wall scan.

Reproducibility

The 3D cross-sectional aortic vessel wall images of the aortic vessel wall acquired with respiratory motion suppression were also analyzed using the VesselMASS software package (23). Inner and outer wall contours were determined using an automated vessel wall contour detection algorithm as previously described (24), without the use of gray level stretching. The center of the aorta was localized manually per interactive mouse-click in each slice and the contours were manually adapted in regions where the contours could not be detected adequately by the algorithm. The circumference of both the inner and outer wall in all slices was divided into 12 equiangular segments. Subsequently, the mean percentage and location of the segments (average of the analyzed slices) in which the inner or outer wall contour needed adjustment was registered for each 3D cross-sectional vessel wall scan. The mean VWT per slice, vessel lumen area (VLA), and the area defined by the outer wall contour (vessel outer wall area [VOA]) were also computed. The vessel wall area (VWA) was calculated by subtracting the VLA from the VOA. Vessel wall volume (VWV) was computed by multiplying the VWA with the slice thickness and the total number of slices.

The 3D cross-sectional vessel wall scans obtained during the two successive examinations in the 10 volunteers were analyzed by observer 1 (S.R.) (the 3D cross-sectional vessel wall scan in the first examination is considered the reference standard). Subsequently, the analyses of the first 3D cross-sectional scans were repeated by observer 1, 1 week later in a blinded manner to assess intraobserver variability. In addition, observer 2 (J.W.) performed the analyses in these scans to evaluate interobserver variability.

Further, the VLA and the VWT measured in the second to last caudal slice (slice 2) and the most cranial slice (slice 10) of the cross-sectional 3D dataset, were compared to evaluate the effectiveness of the 3D dual inversion prepulse, since insufficient blood suppression may lead to artifactual vessel wall thickening due to slow-flowing blood near the edge of the vessel wall. This effect is expected to be most pronounced for the caudal slices (downstream in the descending aorta) and is a concern for 3D volumetric DIR acquisitions. Slice 2 was evaluated since the signal from the vessel wall was suboptimal in the most caudal slice (slice 1) in all scans (slice profile), and was therefore excluded from the analysis. SNR and wall-lumen CNR were measured as described above.

Furthermore, by consensus reading, 2 observers (S.R. and J.W.) visually evaluated the extent to which the outer wall boundary of the vessel wall could not be differentiated from adjacent tissue. The circumference of the outer wall boundary was divided into 12 equiangular segments as described above, and the mean percentage and location of segments (averaged of the analyzed slices) for which the outer wall could not be visually discriminated was computed.

Statistical analysis
Continuous data are expressed as mean ± SD. Data from the different measurements were compared using the paired *t*-test. The correlation between the VWV measurements of the reference standard and the repeated measurements of observer 1, and the measurements of the second vessel wall scan and the measurements of observer 2 were assessed using Pearson's correlation coefficient (r). Furthermore, the intraclass correlations coefficient (ICC) for absolute agreement was calculated to assess intraobserver, interobserver and interscan agreement, and the coefficient of variance (CV) was determined. The CV was defined as the SD of the differences between the two series of measurements divided by the mean of both measurements. Furthermore, Bland-Altman plots were computed.

In addition, the final (adjusted) contours of the repeated segmentation by observer 1 and the segmentation by observer 2 were compared with the reference standard. The results of the comparison were expressed as the degree of similarity (S), defined as the percentage of points that are similar between two contours following the equation (25):

$$S(\%) = (\sum_{n=1}^{N} p_n(d) / N) * 100\%$$ [1]

with

$$p_n(d) = 1 \ if \ d \le T, 0 \ if \ d > T$$ [2]

In Eqs. [1] and [2], d is the distance between each pair of corresponding points on the two contour sets that are being compared. N is the number of points per contour (N = 100), and T is the distance threshold. Pairs of corresponding points are assumed to be similar if the distance does not exceed the threshold value T. The reconstructed pixel size is 0.53 × 0.53 mm. Consequently, on average, the distance from a point on a contour set to the next pixel would be 0.265 mm, and T was set to 0.265 mm.

Results

The MRI examinations were successfully completed in all subjects. However, as mentioned above, the signal from the vessel wall in the first (most caudal) slice of the 3D cross-sectional aortic vessel wall scan was suboptimal in all subjects, therefore, this first slice of each 3D cross-sectional vessel wall scan was excluded from the analysis.

Respiratory navigator
The heart rate of the subjects, examined in order to test the effect of respiratory motion suppression on image quality, was similar during the 3D cross-sectional vessel wall scans performed with and without respiratory navigator (62 ± 6 bpm vs. 63 ± 7 bpm, p = 0.4). The duration of the scans performed with respiratory navigator was significantly longer than that without respiratory navigator (6.5 ± 1.0 min vs. 3.3 ± 0.3 min, p < 0.01). The average navigator gating efficiency was 52 ± 10 %. SNR and wall-lumen CNR were significantly higher in the 3D cross-sectional vessel wall scans performed with respiratory navigator compared with scans obtained without respiratory navigator (15.0 ± 4.6 vs. 12.3 ± 4.0, p = 0.017 and 9.8 ± 3.2 vs. 6.7 ± 1.8, p < 0.01, respectively). Vessel wall sharpness was also superior in the scans performed with respiratory navigator (67 ± 8% vs. 57 ± 7%, p < 0.01). Each 3D cross-sectional vessel wall scan performed without respiratory navigator showed respiratory motion artifacts in the foldover direction, in contrast to scans performed with navigator (Figure 3). Furthermore, the mean extent of nonvisible outer wall contour was higher in scans performed without respiratory navigator (average of all segments of the nine analyzed slices: 36 ± 15 % vs. 24 ± 10 %, p < 0.05) (Figure 4).

Figure 3.
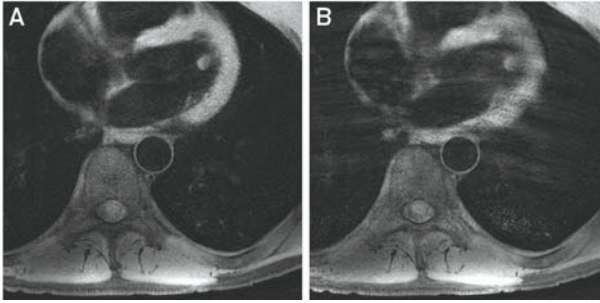
Cross-sectional 3D vessel wall scans performed with (A) and without (B) respiratory navigator.

Figure 4.
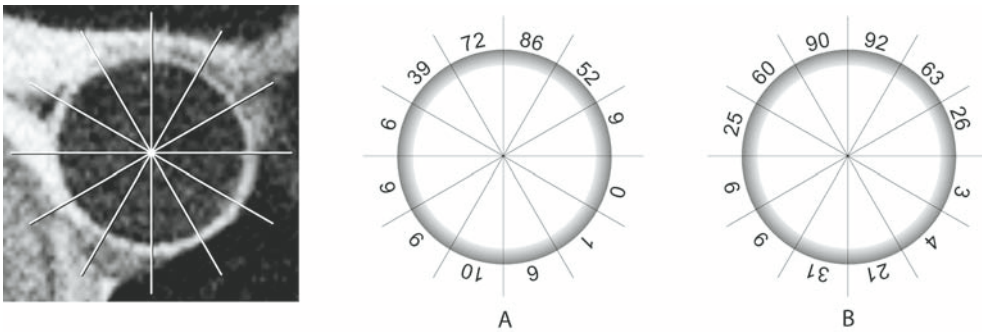
The extent (mean percentage) of nonvisible outer wall contour in the 3D cross-sectional vessel wall scan performed with (A) and without (B) respiratory navigator, presented per segment. The mean percentage per segment is calculated by averaging the data of the nine analyzed slices in the seven adult subjects.

Reproducibility

The average heart rate during the 3D navigator gated cross-sectional vessel wall scans was 61 ± 11 bpm and did not differ between the first and second vessel wall scan (61 ± 11 bpm vs. 62 ± 12 bpm, p = 0.2). The average acquisition time per 3D cross-sectional aortic vessel wall scan was 7.7 ± 3.8 min (7.8 ± 4.5 min vs. 7.6 ± 3.2 min, p = 0.6). The average navigator gating efficiency was 50 ± 14 % and was similar between the first and second scan (51 ± 15% vs. 49 ± 14%, p = 0.5).

The mean percentage and location of segments in which the inner and outer wall contour had to be manually adjusted are presented in Table 1 and Figure 5. No significant difference in location or percentage of adjusted segments between the two scans or between the two observers was found.

Figure 5.
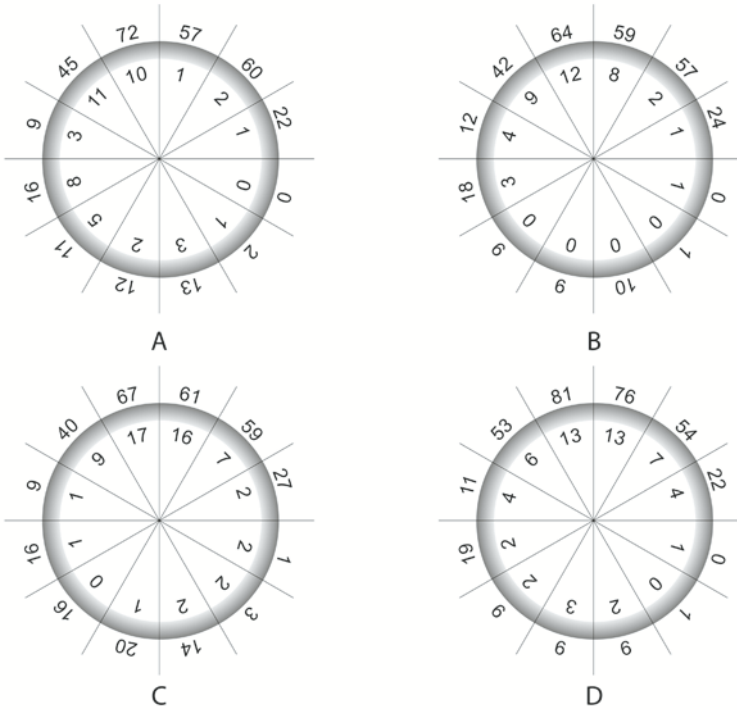
The extent (mean percentage) of manual inner and outer wall contour adjustments needed after automated contour detection. The mean percentage per segment is calculated by averaging the data of the nine analyzed slices in the ten adult subjects. The numbers at the inside and outside of the circle correspond to the inner and outer wall contour, respectively.
A. Scan 1: observer 1 (reference standard), B. Scan 1: repeated analysis observer 1, C. Scan 2: observer 1, D. Scan 1: observer 2

Table 1. Percentage of inner and outer wall contours that needed manual adjustment after automated contour detection.

	Inner wall contour (%)	Outer wall contour (%)
Scan 1: observer 1 (reference standard)	3.9 ± 4.5	26.6 ± 12.8
Scan 1: observer 1 (repeated segmentation)	3.3 ± 4.5	24.4 ± 11.1
Scan 2: observer 1	5.2 ± 6.6	28.8 ± 17.1
Scan 1: observer 2	5.0 ± 5.5	28.7 ± 11.5

Data are presented as mean ± SD.

The mean VWV derived from the first 3D cross-sectional vessel wall scan analyzed by observer 1 (reference standard) was 1.42 ± 0.26 mm³. The repeated evaluation of the first scan by observer 1 resulted in a mean VWV of 1.42 ± 0.24 mm³ (p = 0.6 vs. reference standard).

The VWV observed by observer 1 in the second scan was similar to the reference standard (1.44 ± 0.25 mm³, p = 0.4). A small but significant difference was identified between the VWV calculated by observer 2 and the reference standard (1.34 ± 0.26 mm³ vs. 1.42 ± 0.26 mm³, p < 0.05). Scatter diagrams of the VWV measurements are shown in Figure 6.

Figure 6.
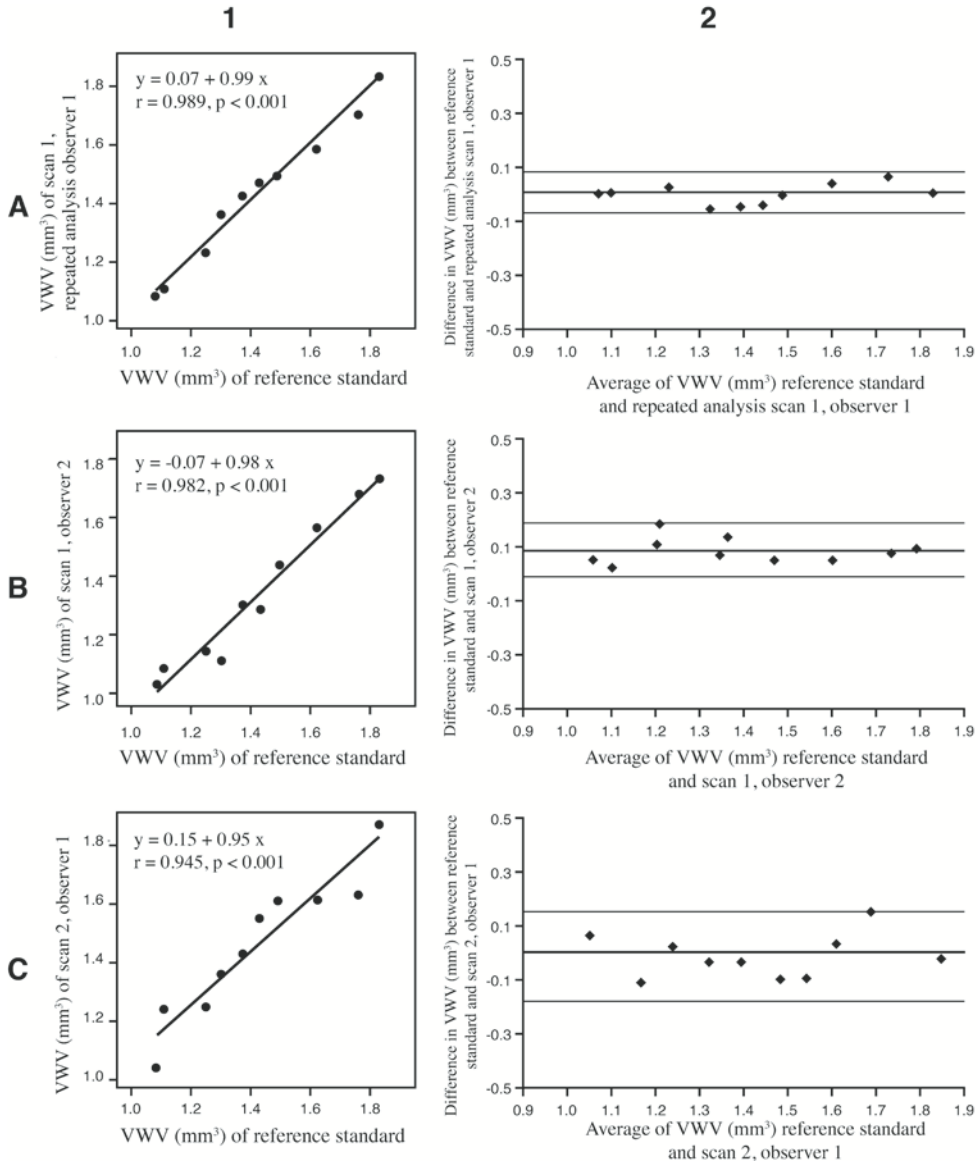
Scatter diagrams (1) and Bland-Altman plots (2) of the VWV (mm³) measurements performed by observer 1 in scan 1 (reference standard) compared with repeated analysis of scan 1 by observer 1 (A), scan 1 by observer 2 (B), and scan 2 by observer 1 (C).

A highly significant correlation in VWV was observed between the reference standard and the repeated measurements of observer 1 ($r = 0.989$, $p < 0.001$) and between the reference standard and observer 2 ($r = 0.982$, $p < 0.001$), and the second scan ($r = 0.945$, $p < 0.001$). The ICC for VWV concerning intraobserver agreement was 0.99. The ICCs describing interobserver and interscan agreement were 0.94 and 0.95, respectively. The CV was 2.3% for intraobserver analysis, 3.5% for interobserver analysis and 5.8% for interscan analysis. Bland-Altman plots are presented in Figure 6. The mean degrees of similarity between the repeated segmentation of observer 1 and the segmentation of observer 2 compared to the reference standard were excellent for inner wall contours as well as for outer wall contours (Table 2).

Table 2. Interobserver and intraobserver degree of similarity for inner and outer wall contours.

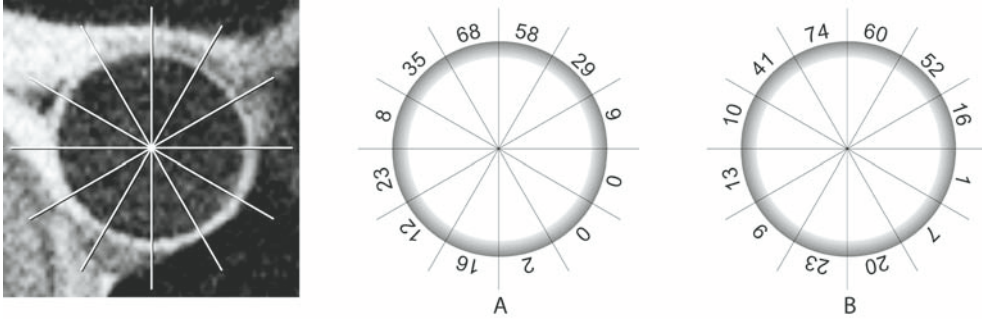|	Inner wall contour	Outer wall contour
Intraobserver similarity (%)	88.2 ± 4.3	85.6 ± 4.7
Interobserver similarity (%)	85.7 ± 9.3	83.2 ± 6.0

Data are presented as mean ± SD.

The mean aortic VLA significantly decreased from cranial to caudal between the two outer slices (slice 2 and slice 10) of the 3D cross-sectional vessel wall scan, whereas the vessel wall thickness between these two slices was similar (Table 3).

SNR of the vessel wall and wall-lumen CNR were similar in the first and second 3D cross-sectional vessel wall scan (13.8 ± 2.5 vs. 12.8 ± 2.9, $p = 0.3$ and 8.2 ± 2.0 vs. 7.9 ± 2.0, $p = 0.6$, respectively).

The mean percentage of the outer wall contour that could not be discriminated from adjacent tissue was 22 ± 9 % in the first cross-sectional 3D vessel wall scan and 27 ± 14% ($p = 0.4$) in the second scan. The location of these segments in which the outer wall boundary could not adequately be identified is presented in Figure 7. Differentiation between the outer wall boundary and adjacent tissue appeared to be the most difficult in the anterior part of the aorta. In these anterior segments, differentiation between the aortic outer wall boundary and adjacent tissue was not possible in 58% to 74%. In this region, the aorta directly borders the left atrium and the left pulmonary vein. In addition, connective tissue, subcarinal glands, the esophagus and the vena azygos are difficult to discriminate from the right border of the aortic vessel wall. These tissues seem to have the same signal intensity as the vessel wall on our T_1-weighted images.

Figure 7.

The extent (mean percentage) of nonvisible outer wall contour in the first (A) and second (B) 3D cross-sectional vessel wall scan, presented per segment. The mean percentage per segment is calculated by averaging the data of the nine analyzed slices in the ten adult subjects.

Discussion

In the present study, we have implemented a respiratory motion suppressed free-breathing 3D DIR segmented k-space gradient echo imaging sequence at 3T for reproducible aortic vessel wall dimension measurements. A standardized scan protocol was used to ensure accurate co-registration of the imaged slice position for serial scanning sessions. The effects of respiratory motion suppression on image quality were studied and the reproducibility of quantitative aortic vessel wall dimension measurements was evaluated. The results demonstrate that respiratory motion suppression with navigators substantially improves image quality. Furthermore, good reproducibility between the repeated scans acquired with respiratory motion suppression was demonstrated and the interobserver and intraobserver agreement of the aortic vessel wall measurements was excellent.

A small but significant difference was observed between the reference standard and the measurements of observer 2. However, this difference was very small-in the order of 5%, which means a mismatch of approximately 14 voxels out of the 282 voxels per vessel wall area per slice. Furthermore, the high ICC and the excellent degree of similarity of the inner and outer wall contours drawn by the different observers reflect good reproducibility.

The visual assessment of the outer wall contour demonstrated that mainly the anterior part could not be easily discriminated. In this region, anatomical structures adjacent to the aortic vessel wall have a very similar signal intensity. The outer wall contour in this region had to be extrapolated and differences in these extrapolations may contribute to the differences in VWV observed between the first segmentation of observer 1 and the segmentation of observer 2.

The scan reproducibility of aortic vessel wall measurements was previously demonstrated in asymptomatic adult subjects and in patients with CAD (7,8). Those and other previous

Table 3. Aortic vessel wall measurements in the cranial (slice 10) vs. caudal slices (slice 2) of the 3D cross-sectional vessel wall scan.

	Cranial slice	Caudal slice	P-value
Lumen area (cm²)			
Scan 1: observer 1 (reference standard)	2.97 ± 0.78	2.88 ± 0.76	0.017
Scan 1: observer 1 (repeated analysis)	2.97 ± 0.78	2.87 ± 0.76	0.007
Scan 2: observer 1	2.98 ± 0.76	2.90 ± 0.75	0.005
Scan 1: observer 2	2.96 ± 0.78	2.86 ± 0.77	0.009
Outer wall area (cm²)			
Scan 1: observer 1 (reference standard)	3.79 ± 0.93	3.64 ± 0.86	0.022
Scan 1: observer 1 (repeated analysis)	3.78 ± 0.91	3.63 ± 0.86	0.013
Scan 2: observer 1	3.81 ± 0.92	3.67 ± 0.83	0.005
Scan 1: observer 2	3.73 ± 0.93	3.61 ± 0.9	0.013
Vessel wall area (cm²)			
Scan 1: observer 1 (reference standard)	0.83 ± 0.17	0.76 ± 0.12	0.12
Scan 1: observer 1 (repeated analysis)	0.81 ± 0.16	0.76 ± 0.12	0.12
Scan 2: observer 1	0.83 ± 0.17	0.77 ± 0.11	0.047
Scan 1: observer 2	0.78 ± 0.17	0.73 ± 0.12	0.17
Vessel wall thickness (cm)			
Scan 1: observer 1 (reference standard)	1.27 ± 0.14	1.19 ± 0.11	0.12
Scan 1: observer 1 (repeated analysis)	1.26 ± 0.15	1.19 ± 0.10	0.31
Scan 2: observer 1	1.28 ± 0.13	1.20 ± 0.12	0.074
Scan 1: observer 2	1.20 ± 0.14	1.15 ± 0.09	0.29

MRI studies relied on 1.5T MRI systems for evaluation of the aortic vessel wall, with in-plane spatial resolutions ranging from 1.03 × 0.64 mm to 0.78 × 0.78 mm with slice thickness of 4-5 mm (2,4,10,26). However, the use of 3T MRI systems offers potential since the higher SNR as a result of the stronger magnetic field can be traded for a higher spatial resolution (9). Thus, we sought to implement a black-blood aortic vessel wall imaging sequence with an in–plane resolution of 0.53 × 0.55 mm and a slice thickness of 4 mm. As a result, the volume of one acquired voxel was 1.17 mm³, which is smaller than that reported in previous studies using 1.5T (ca. 2.5 mm³ or larger)(6,10,27). However, imaging with higher spatial resolution necessitates adequate motion suppression of both intrinsic aortic motion and respiratory motion. Acquiring data during the period of slow aortic flow (diastole) minimizes the effect of intrinsic aortic motion (8,10). In all previous 1.5T

aortic vessel wall studies, data acquisition was performed during free-breathing or during breath-holds. However, imaging with superior in-plane resolution does not allow for data acquisition during free-breathing since respiratory motion will deteriorate image quality. Also, using breath-hold data acquisition, residual respiratory motion may be caused by cranial diaphragmatic drift (28) during a sustained breath-hold, and the diaphragmatic and cardiac positions frequently vary by up to 1 cm among serial breath-holds (29). Furthermore, the breath-hold duration may not easily be tolerated by all the patients. Thus, in the present study, respiratory navigator technology was used to support imaging at such a high spatial resolution and the superior SNR, CNR, vessel sharpness, reduced motion artifacts, and superior delineation of the outer vessel wall in scans performed with respiratory navigator compared to scans without respiratory navigator indicate the additive value of motion suppression on image quality. This advantage clearly comes at the expense of a twofold increase in scanning time. This has to be considered for the design of patient studies using this technology. However, the improved image quality and improved boundary definition of the vessel wall support imaging at a higher spatial resolution which may lead to a more accurate measurement of small changes in vessel wall dimensions. This has important implications for the sample size definition in studies in which changes in vessel wall dimensions as a result of atherosclerosis progression or in response to interventions (30) are quantitatively investigated.

At the present time, black-blood aortic vessel wall imaging at 1.5T is typically performed using 2D T_2-weighted or proton density-weighted DIR fast spin echo (FSE) sequences (2,4,10,31,32). However, the increased specific absorption rate (SAR), prolonged T_1 and increased B_1-inhomogeneity (33) at higher magnetic field strength may adversely affect FSE imaging. In addition, during the developmental phase of this protocol and based on previous work on carotid imaging (34), both conspicuity and wall-lumen contrast were superior on segmented k-space gradient echo images when compared to FSE. Therefore, and for the measurement of vessel wall dimensions, the focus was on the development of a high-spatial resolution gradient echo imaging technique. However, for the identification of different plaque components, segmented k-space gradient echo imaging may not be sufficient and the combination with additional prepulses for contrast generation remains to be investigated. Nevertheless, it is anticipated that FSE imaging would equally benefit from navigators for respiratory motion suppression.

Three-dimensional imaging has advantages when compared to 2D imaging as it allows for improved SNR and therefore higher spatial resolution (35). Previous studies demonstrated the feasibility of 3D coronary vessel wall imaging in healthy subjects and patients (35,36). For aortic vessel wall imaging, Koktzoglou and Li implemented a 3D diffusion prepared gradient echo sequence at 1.5T and demonstrated an improved aortic wall-lumen CNR compared to 2D T_2-weighted DIR FSE technique (37). To our knowledge, the present study is the first to describe the use of a navigator-gated 3D DIR segmented k-space gradient echo imaging for aortic vessel wall dimension measurements at 3T.

To evaluate the effectiveness of the dual inversion prepulse for signal-nulling of the blood pool, we compared the VLA and VWT in two of the most peripheral slices of the 3D volume. As shown in the literature, the diameter of the aorta gradually tapers from the proximal to the distal descending thoracic aorta (38), whereas the VWT values in the proximal and distal thoracic aorta are very similar (39). This is in accordance with our study, in which the VLA decreased from cranial to caudal while simultaneously the VWT in these two outer slices was very similar or even decreased towards the most caudal slice. These findings suggest that suboptimal suppression of the signal from slow-flowing blood near the vessel wall may not be a limitation for the currently used slab thickness. However, this remains to be confirmed in patients with aneurysms and flow-limiting stenoses.

Motion-suppressed 3D black-blood vessel wall imaging with high spatial resolution at 3T is a robust and reproducible technique that may support detection of arterial wall thickening preceding luminal narrowing (5). In addition, the high spatial resolution may enable more precise evaluation of the effect of lifestyle changes or medical treatment on changes in wall thickness, particularly when data analysis is performed by the same observer at baseline and follow-up. The high reproducibility of the aortic vessel wall scans presented in this study enables detection of 8% regression in vessel wall volume during follow-up, which can be expected after lipid-lowering therapy within 12 months (30), using a sample size of only 8 patients with a 90% power at the alpha level of 0.05 (sample size calculation based on two-sided paired *t*-test)(40).

Limitations of the present study include the fact that this methodology was only tested in healthy adult subjects, and further studies in patients with advanced atherosclerosis are needed to verify the robustness of this MRI protocol. Furthermore, since one of the main purposes of this study was to test the interscan reproducibility, the total scan protocol had to be performed twice. Due to time constraints, we choose to image 2 cm of the thoracic aorta in cross-sectional view only. However, coverage of a more extensive part of the aorta by acquiring multiple 3D slabs may be clinically useful. Alternatively, and rather than acquiring serial 3D volumes for enhanced coverage, a larger 3D slab could be acquired. However, this approach increases the likelihood that slow flow leads to artifactual augmentation of VWT measurements for the more caudal slices.

In conclusion, the 3T motion suppressed 3D DIR segmented k-space gradient echo imaging sequence as evaluated in this study enables the assessment of the aortic vessel wall with high spatial resolution, and the use of a respiratory navigator substantially improves image quality at the expense of a twofold increase in scanning time. The high intraobserver, interobserver and interscan reproducibility warrant the use of this technique in longitudinal studies with and without intervention.

Acknowlegdements

We thank Michael Schär from Philips Healthcare (Cleveland, OH, USA) and Johns Hopkins University School of Medicine (Baltimore, MD, USA) for his technical support with the shimming tool.

References

1. Fuster V, Fayad ZA, Badimon JJ. Acute coronary syndromes: biology. Lancet 1999;353 Suppl 2:SII5-SII9.

2. Taniguchi H, Momiyama Y, Fayad ZA, et al. In vivo magnetic resonance evaluation of associations between aortic atherosclerosis and both risk factors and coronary artery disease in patients referred for coronary angiography. Am Heart J 2004;148:137-143.

3. Solberg LA, Strong JP. Risk factors and atherosclerotic lesions. A review of autopsy studies. Arteriosclerosis 1983;3:187-198.

4. Jaffer FA, O'Donnell CJ, Larson MG, et al. Age and sex distribution of subclinical aortic atherosclerosis: a magnetic resonance imaging examination of the Framingham Heart Study. Arterioscler Thromb Vasc Biol 2002;22:849-854.

5. Glagov S, Weisenberg E, Zarins CK, et al. Compensatory enlargement of human atherosclerotic coronary arteries. N Engl J Med 1987;316:1371-1375.

6. Corti R, Fuster V, Fayad ZA, et al. Lipid lowering by simvastatin induces regression of human atherosclerotic lesions: two years' follow-up by high-resolution noninvasive magnetic resonance imaging. Circulation 2002;106:2884-2887.

7. Chan SK, Jaffer FA, Botnar RM, et al. Scan reproducibility of magnetic resonance imaging assessment of aortic atherosclerosis burden. J Cardiovasc Magn Reson 2001;3:331-338.

8. Li AE, Kamel I, Rando F, et al. Using MRI to assess aortic wall thickness in the multiethnic study of atherosclerosis: distribution by race, sex, and age. Am J Roentgenol 2004;182:593-597.

9. Wen H, Denison TJ, Singerman RW, et al. The intrinsic signal-to-noise ratio in human cardiac imaging at 1.5, 3, and 4 T. J Magn Reson 1997;125:65-71.

10. Fayad ZA, Nahar T, Fallon JT, et al. In vivo magnetic resonance evaluation of atherosclerotic plaques in the human thoracic aorta: a comparison with transesophageal echocardiography. Circulation 2000;101:2503-2509.

11. McConnell MV, Khasgiwala VC, Savord BJ, et al. Comparison of respiratory suppression methods and navigator locations for MR coronary angiography. Am J Roentgenol 1997;168:1369-1375.

12. Oshinski JN, Hofland L, Mukundan S Jr, et al. Two-dimensional coronary MR angiography without breath holding. Radiology 1996;201:737-743.

13. Koops A, Ittrich H, Petri S, et al. Multicontrast-weighted magnetic resonance imaging of atherosclerotic plaques at 3.0 and 1.5 Tesla: ex-vivo comparison with histopathologic correlation. Eur Radiol 2007;17:279-286.

14. Harloff A, Dudler P, Frydrychowicz A, et al. Reliability of aortic MRI at 3 Tesla in patients with acute cryptogenic stroke. J Neurol Neurosurg Psychiatry 2008;79:540-546.

15. Markl M, Dudler P, Fydrychowicz A, et al. Optimized 3D bright blood MRI of aortic plaque at 3 T. Magn Reson Imaging 2008;26:330-336.

16. Schär M, Kozerke S, Fischer SE, et al. Cardiac SSFP imaging at 3 Tesla. Magn Reson Med 2004;51:799-806.

17. Stuber M, Botnar RM, Danias PG, et al. Double-oblique free-breathing high resolution three-dimensional coronary magnetic resonance angiography. J Am Coll Cardiol 1999;34:524-531.

18. Edelman RR, Chien D, Kim D. Fast selective black blood MR imaging. Radiology 1991;181:655-660.

19. Fleckenstein JL, Archer BT, Barker BA, et al. Fast short-tau inversion-recovery MR imaging. Radiology 1991;179:499-504.

20. McConnell MV, Khasgiwala VC, Savord BJ, et al. Prospective adaptive navigator correction for breath-hold MR coronary angiography. Magn Reson Med 1997;37:148-152.

21. Etienne A, Botnar RM, Van Muiswinkel AM, et al. "Soap-Bubble" visualization and quantitative analysis of 3D coronary magnetic resonance angiograms. Magn Reson Med 2002;48:658-666.

22. Botnar RM, Stuber M, Danias PG, et al. Improved coronary artery definition with T2-weighted, free-breathing, three-dimensional coronary MRA. Circulation 1999;99:3139-3148.

23. Adame IM, van der Geest RJ, Wasserman BA, et al. Automatic segmentation and plaque characterization in atherosclerotic carotid artery MR images. MAGMA 2004;16:227-234.

24. Adame IM, van der Geest RJ, Bluemke DA, et al. Automatic vessel wall contour detection and quantification of wall thickness in in-vivo MR images of the human aorta. J Magn Reson Imaging 2006;24:595-602.

25. Angelie E, de Koning PJ, Danilouchkine MG, et al. Optimizing the automatic segmentation of the left ventricle in magnetic resonance images. Med Phys 2005;32:369-375.

26. Yonemura A, Momiyama Y, Fayad ZA, et al. Effect of lipid-lowering therapy with atorvastatin on atherosclerotic aortic plaques detected by noninvasive magnetic resonance imaging. J Am Coll Cardiol 2005;45:733-742.

27. Corti R, Fuster V, Fayad ZA, et al. Effects of aggressive versus conventional lipid-lowering therapy by simvastatin on human atherosclerotic lesions: a prospective, randomized, double-blind trial with high-resolution magnetic resonance imaging. J Am Coll Cardiol 2005;46:106-112.

28. Danias PG, Stuber M, Botnar RM, et al. Navigator assessment of breath-hold duration: impact of supplemental oxygen and hyperventilation. Am J Roentgenol 1998;171:395-397.

29. Liu YL, Riederer SJ, Rossman PJ, et al. A monitoring, feedback, and triggering system for reproducible breath-hold MR imaging. Magn Reson Med 1993;30:507-511.

30. Corti R, Fayad ZA, Fuster V, et al. Effects of lipid-lowering by simvastatin on human atherosclerotic lesions: a longitudinal study by high-resolution, noninvasive magnetic resonance imaging. Circulation 2001;104:249-252.

31. Kim WY, Astrup AS, Stuber M, et al. Subclinical coronary and aortic atherosclerosis detected by magnetic resonance imaging in type 1 diabetes with and without diabetic nephropathy. Circulation 2007;115:228-235

32. Momiyama Y, Kato R, Fayad ZA, et al. A possible association between coronary plaque instability and complex plaques in abdominal aorta. Arterioscler Thromb Vasc Biol 2006;26:903-909.

33. Dougherty L, Connick TJ, Mizsei G. Cardiac imaging at 4 Tesla. Magn Reson Med 2001;45:176-178.

34. Alizadeh DR, Doornbos J, Tamsma JT, et al. Assessment of the carotid artery by MRI at 3T: a study on reproducibility. J Magn Reson Imaging 2007;25:1035-1043.

35. Botnar RM, Kim WY, Bornert P, et al. 3D coronary vessel wall imaging utilizing a local inversion technique with spiral image acquisition. Magn Reson Med 2001;46:848-854.

36. Kim WY, Stuber M, Bornert P, et al. Three-dimensional black-blood cardiac magnetic resonance coronary vessel wall imaging detects positive arterial remodeling in patients with nonsignificant coronary artery disease. Circulation 2002;106:296-299.

37. Koktzoglou I, Li D. Diffusion-prepared segmented steady-state free precession: Application to 3D black-blood cardiovascular magnetic resonance of the thoracic aorta and carotid artery walls. J Cardiovasc Magn Reson 2007;9:33-42.

38. Goss CM. Gray's anatomy. 1996. Lea & Febiger, Philidelphia.

39. Bezerra Lira-Filho E, Campos O, Lazaro AJ, et al. Thoracic aorta evaluation in patients with Takayasu's arteritis by transesophageal echocardiography. J Am Soc Echocardiogr 2006;19:829-834.

40. Lenth RV. Some Practical Guidelines for Effective Sample Size Determination. The American Statistician 2001;55:187-193.

2

Chapter